CPTNP-2025-042

Parameter Inference from Final-State Entanglement in Higgs Decays

Jia Liu,[1,2,*] Masanori Tanaka,[2,†] Xiao-Ping Wang,[3,‡] Jing-Jun Zhang,[1,§] and Zifan Zheng[1,¶]

[1] *School of Physics and State Key Laboratory of Nuclear Physics and Technology, Peking University, Beijing 100871, China*
[2] *Center for High Energy Physics, Peking University, Beijing 100871, China*
[3] *School of Physics, Beihang University, Beijing 100083, China*

The decay out-states of unstable Standard Model (SM) particles provide a unique, well-defined intrinsic quantum-information probe of the SM parameter space. We use Higgs decays as a test case: after tracing out kinematics, we compute entanglement among final-state spins and colors across all decay channels and impose a near-maximal entanglement-entropy criterion. This criterion yields quantitative indications for fundamental parameters. Within the SM, the entanglement entropy exhibits a global maximum close to the observed Higgs mass and the measured W mass, the latter being equivalent to the $SU(2)_L$ gauge coupling. In a two-parameter kappa framework, applying the same criterion points to an SM-like balance between vector and fermion couplings, constraining the ratio of the sector-wide rescalings. These results suggest that entanglement extremality can serve as a complementary handle on fundamental parameters.

INTRODUCTION

Quantum-information ideas are increasingly applied to particle physics. Since Bell's proposal of experimentally testable entanglement [1], the possibility of probing quantum correlations in fundamental interactions has been widely explored [2]. Observations of spin entanglement in top–quark pairs at the LHC [3, 4] have opened a possibility that colliders can probe entanglement directly, establishing quantum-information observables as a viable probe in high-energy physics [5–7].

Recent studies probe whether quantum-information extrema encode Standard Model (SM) parameters. Examples include maximal helicity entanglement in lepton annihilation/scattering yielding $\sin^2\theta_W = 1/4$ [8], minimized entanglement in neutrino oscillations constraining the PMNS CP phase [9], and minimized flavor-entanglement power shaping CKM and PMNS mixing [10]. Magic–based QED criteria further refine θ_W inferences [11]. Related studies link entanglement to symmetries and dynamics [12–26].

The Higgs boson underlies electroweak symmetry (EW) breaking and the origin of particle masses. While its properties have been extensively measured at colliders [27, 28], its mass remains a free SM parameter without a universally accepted theoretical explanation. Several approaches aim to explain it: asymptotic-safety arguments in the SM coupled to gravity suggest $m_h \simeq 126$ GeV [29], criticality of the Higgs potential yields $m_h \sim 135\pm 9$ GeV [30], and Planck-scale mass sum rules predict $m_h \sim 135$ GeV [31]. Additionally, a maximal classical multinomial entropy constructed from the Higgs decay branching ratios yields $m_h = 125.04 \pm 0.25\,\text{GeV}$ [32].

In this work, we infer SM parameters from the decay products of unstable particles. Complementary to scattering analyses, which require a specified center-of-mass energy, scattering angle and a two-particle in-state, decays are kinematically fixed in the parent's rest frame and start from a single-particle in-state determined by the SM spectrum. This makes decay out-states an intrinsic and minimal quantum probe for quantum-information studies in particle physics.

We focus on Higgs decays as a test case, analyzing kinematics and evaluating final-state entanglement in spin and color. The Higgs decays are a promising process that may serve as a laboratory for quantum-information tests, with studies of Bell inequalities and entanglement signatures across multiple channels [33–47]. By considering all accessible decay channels, rather than a single exclusive mode, we link our observable directly to the Higgs mass, EW gauge couplings, and Yukawa couplings. A near-maximal entropy criterion then provides insights into these parameters: within the SM it selects Higgs and W masses close to their observed values. In a two-parameter κ framework, it prefers an approximately SM-like balance between vector and fermion couplings. This method is general, directly tied to measurable decay patterns, and extends naturally to other unstable particles beyond the Higgs boson.

THE DECAY OUT-STATE OF UNSTABLE PARTICLES

An unstable particle such as the Higgs boson is prepared in a one-particle in-state. At the rest frame, it is given by

$$|\text{in}\rangle = \mathcal{N}^{-1}\,|\mathbf{p}_{\text{in}}\rangle\,|\lambda_{\text{in}}\rangle\ , \tag{1}$$

where $|\mathbf{p}_{\text{in}}\rangle$ denotes a one-particle momentum eigenstate and $|\lambda_{\text{in}}\rangle$ collects intrinsic quantum numbers (spin/helicity and gauge charges). The normalization factor $\mathcal{N} = (2E_{\text{in}}\mathcal{V})^{1/2}$ ensures $\langle\text{in}|\text{in}\rangle = 1$ with $\langle\mathbf{p}|\mathbf{p}'\rangle = 2E_{\text{in}}(2\pi)^3\delta^{(3)}(\mathbf{p}_{\text{in}} - \mathbf{p}'_{\text{in}})$ and the box normalization $(2\pi)^3\delta^{(3)}(\mathbf{0}) = \mathcal{V}$. For a scalar field, the spin label λ_{in} is absent. After the decay, the out-state is

$$|\text{out}\rangle = i\hat{T}\,|\text{in}\rangle\ , \tag{2}$$

with $\hat{T}$ is the transition operator. We neglect the trivial identity piece in the S-matrix, $S = 1 + i\hat{T}$, since we focus on the entanglement specifically generated *by the decay.*

For two-body decays, the T-matrix element is related to the invariant amplitude $\mathcal{M}$ by

$$\begin{aligned}&\langle \mathbf{p}_1\mathbf{p}_2; s_1 s_2; c_1 c_2; ij\,| i\hat{T} |\mathbf{p}_{\rm in}, \lambda_{\rm in}\rangle \\ &\quad = (2\pi)^4 \delta^4(p_{\rm in} - p_1 - p_2) i \mathcal{M}^{c_1 c_2;\, ij}_{s_1 s_2}(p_{\rm in} \to p_1 p_2)\,,\end{aligned} \tag{3}$$

where $|s_\alpha\rangle$ and $|c_\alpha\rangle$ ($\alpha = 1, 2$) label spin/helicity and color states, and $|i, j\rangle$ labels the particle species in the final state. For Higgs decays, the initial particle carries neither color nor spin. Color conservation implies $c_2 = \overline{c_1}$, so we use $\mathcal{M}^{c_1 c_2;\, i,j}_{s_1 s_2} \to \mathcal{M}^{c_1;\, i,j}_{s_1 s_2}$ below. The out-state can then be written in terms of amplitudes as

$$\begin{aligned}|{\rm out}\rangle = \frac{1}{\mathcal{N}} \sum_{i,j} \sum_{s_1 s_2} \sum_{c} \int d\Pi_1 d\Pi_2 (2\pi)^4 \delta^4(p_{\rm in} - p_1 - p_2) \\ \times \mathcal{M}^{c;\, ij}_{s_1 s_2}(p_{\rm in} \to p_1 p_2)\, |\mathbf{p}_1 \mathbf{p}_2; s_1 s_2; c\bar{c}; ij\rangle\,,\end{aligned} \tag{4}$$

with $d\Pi_i \equiv d^3\mathbf{p}_i/[2E_i(2\pi)^3]$. From Eq. (4), the normalized density matrix of the final state is

$$\rho_f = \frac{|{\rm out}\rangle\langle {\rm out}|}{\langle {\rm out}|{\rm out}\rangle}\,, \tag{5}$$

with

$$\langle {\rm out}|{\rm out}\rangle = \frac{(2\pi)^4\delta^4(0)}{\mathcal{N}^2} 2 m_{\rm in} \Gamma_{\rm tot} = T\Gamma_{\rm tot}\,, \tag{6}$$

where $\delta(0)$ is the delta function reflecting the plane-wave normalization for momentum eigenstates, $m_{\rm in}$ is the mass of the decaying particle, and $\Gamma_{\rm tot}$ is its total decay width. Here we use the standard box-normalization replacement $(2\pi)\delta(0) \to T$.

ENTANGLEMENT ENTROPY FROM DECAYS

We quantify entanglement in the decay out-state using the entanglement entropy (EE), following the formulations in Refs. [48, 49]. We take the bipartition of final states as $\mathcal{H}_{\rm tot} = \mathcal{H}_A \otimes \mathcal{H}_B$, with

$$\mathcal{H}_A = \mathcal{H}^a_{\rm spin} \otimes \mathcal{H}^a_{\rm color} \otimes \mathcal{H}^a_{\rm particle}\,, \tag{7}$$

$$\mathcal{H}_B = \mathcal{H}^a_{\rm kin} \otimes \mathcal{H}^b_{\rm kin} \otimes \mathcal{H}^b_{\rm spin} \otimes \mathcal{H}^b_{\rm color} \otimes \mathcal{H}^b_{\rm particle}\,, \tag{8}$$

where $\mathcal{H}^i_{\rm kin}$, $\mathcal{H}^i_{\rm spin}$, $\mathcal{H}^i_{\rm color}$, and $\mathcal{H}^i_{\rm particle}(i = a, b)$ denote the momentum, spin, color, and particle-type Hilbert spaces for particles i. The reduced density matrix can be got from the total density matrix ρ by tracing out $\mathcal{H}_B$

$$\rho_R = {\rm tr}_{\mathcal{H}_B}[\rho]\,, \tag{9}$$

and we adopt the linear entropy (Tsallis-2) as our measure of entanglement [50, 51]:

$$EE(\rho_R) = 1 - {\rm tr}_{\mathcal{H}_A}[\rho_R^2]\,. \tag{10}$$

Applying ρ_f given in Eq. (5) to Eq. (9) , the reduced density matrix becomes

$$\rho_R = \sum_i \sum_{s_1 s_1' s_2} \sum_c \frac{\Gamma^{cc;\, ii}_{s_1 s_2; s_1' s_2}}{\Gamma_{\rm tot}} |s_1, c, i\rangle\langle s_1', c, i|\,, \tag{11}$$

where

$$\Gamma^{c_1 c_2;\, ij}_{s_1 s_2; s_3 s_4} \equiv \int \frac{d\Phi_2(p_1, p_2)}{2 m_{\rm in}} \sum_k \mathcal{M}^{c_1;\, ik}_{s_1 s_2} (\mathcal{M}^{c_2;\, jk}_{s_3 s_4})^*\,, \tag{12}$$

with $d\Phi_2(p_1, p_2) \equiv d\Pi_1 d\Pi_2 (2\pi)^4 \delta^4(p_{\rm in} \to p_1, p_2)$. Note ρ_R is block diagonal in color and particle type.

Consequently, the linear EE takes the simple form

$$EE(\rho_R) = 1 - \sum_i \frac{\mathcal{P}_i}{N_c^i} {\rm BR}_i^2\,, \tag{13}$$

where N_c^i and ${\rm BR}_i$ are the color multiplicity and the branching ratio (BR) for species i. Thus, EE includes a $1/N_c$ color suppression, 1/3 for quarks and 1/8 for gluons. The spin factor $\mathcal{P}_i$ is

$$\mathcal{P}_i = \frac{\sum_{s_1 s_2 s_3 s_4} \Gamma^{cc;\, ii}_{s_1 s_2; s_3 s_2} \Gamma^{cc;\, ii}_{s_3 s_4; s_1 s_4}}{\left(\sum_{s_1 s_2} \Gamma^{cc;\, ii}_{s_1 s_2; s_1 s_2}\right)^2}\,. \tag{14}$$

For Higgs decays into fermions, this yields $\mathcal{P}_i = 1/2$.

HIGGS DECAYS IN TWO- AND THREE-BODY CHANNELS

We apply the decay-based entanglement framework to Higgs decays. In the SM, there are 14 Higgs decay channels:

$$h \to q\bar{q}\,,\ \ell\bar{\ell}\,,\ WW\,,\ ZZ\,,\ gg\,,\ \gamma\gamma\,,\ Z\gamma\,, \tag{15}$$

where $q = u, d, c, s, t, b$ and $\ell = e, \mu, \tau$ [52].

When $m_h < 2m_V$, we use the notation V^* indicates an off-shell gauge boson. The VV^* channel is nontrivial for the EE calculation as it yields a three-body final state. Consider $h(p_{\rm in}) \to V(p_1)V^*(q) \to V(p_1)f(p_2)\bar{f}'(p_3)$, with $q = p_2 + p_3$ and $V = W/Z$. The corresponding out-state is

$$\begin{aligned}|{\rm out}\rangle \ni \mathcal{N}^{-1} \sum_{\{ff'\}} \sum_{\lambda_1, s_2, s_2} \int d\Phi_3 \mathcal{M}^{ff',V}_{\lambda_1 s_2 s_3}(p_1, p_2, p_3) \\ \times |\mathbf{p}_1, \lambda_1\rangle_V\, |\mathbf{p}_2, s_2, f\rangle\, |\mathbf{p}_3, s_3, f'\rangle\,,\end{aligned} \tag{16}$$

where $d\Phi_3 = d\Pi_1 d\Pi_2 d\Pi_3 (2\pi)^4 \delta^4(p_{\rm in} - p_1 - p_2 - p_3)$ is the three-body phase space, and $\mathcal{M}^{ff',V}_{\lambda_1 s_2 s_3}(p_1, p_2, p_3)$ is the amplitude, with λ_1 and $s_{2,3}$ parameterizing the helicity states of the on-shell V boson and the fermions [53].

The calculation proceeds analogously to the two-body case. We trace over $\mathcal{H}_B$ defined in Eq. (8), now with the

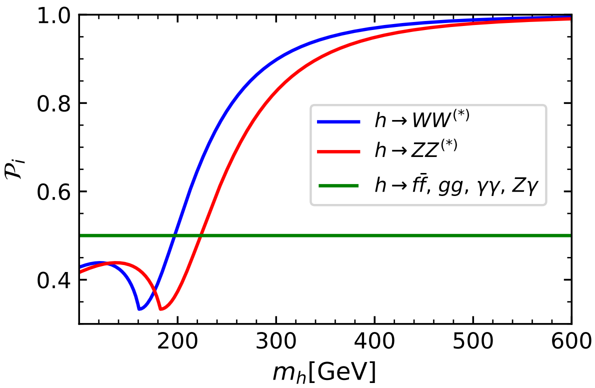

FIG. 1. Spin factors $\mathcal{P}_i$ for each Higgs decay channel as a function of m_h.

understanding that "particle b" encompasses both f and f'. This contributes to the reduced density matrix as

$$\rho_R \ni \sum_{\lambda_1,\lambda_1'} \frac{\Gamma^{VV}_{\lambda_1\lambda_1'}}{\Gamma_{\rm tot}} |\lambda_1\rangle_V \langle\lambda_1'|_V \;, \quad (V=W,Z)\,, \tag{17}$$

where λ_1, λ_1' are the helicities of the on-shell V, and

$$\Gamma^{VV}_{\lambda_1\lambda_1'} = \sum_{\{ff'\}}\sum_{s_2,s_3}\int d\Phi_3 \mathcal{M}^{ff',V}_{\lambda_1 s_2 s_3}\left(\mathcal{M}^{ff',V}_{\lambda_1' s_2 s_3}\right)^* . \tag{18}$$

Thus, the reduced density matrix for the process $h\to VV^*$ has the same structure as in the two-body case, and the subsequent EE analysis can be carried out similarly.

The spin factor $\mathcal{P}^{3-\rm body}_{VV}$ then follows from Eq. (14), see Appendix (App. A) for details,

$$\mathcal{P}^{3-\rm body}_{VV} = \frac{2F_T^2(\epsilon_V)+F_L^2(\epsilon_V)}{[2F_T(\epsilon_V)+F_L(\epsilon_V)]^2}\,, \tag{19}$$

where F_T and F_L encode the transverse and longitudinal helicity contributions,

$$F_T(\epsilon_V) = \int_0^{y_{\rm max}} dy \frac{y}{(y-1)^2}\sqrt{Y-4y}\,, \tag{20}$$

$$F_L(\epsilon_V) = \int_0^{y_{\rm max}} dy \frac{1}{4(y-1)^2} Y\sqrt{Y-4y}\,, \tag{21}$$

with $\epsilon_V = m_h/m_V \in [1,2]$, $Y = (\epsilon_V^2-1-y)^2$ and $y_{\rm max} = (\epsilon_V-1)^2$. Note that $\mathcal{P}_{VV}$ has the same form for the WW and ZZ channels, as the couplings cancel in the ratio. When $m_h \geq 2m_V$, the decay $h\to VV$ is two-body and the spin factor is

$$\mathcal{P}^{2-\rm body}_{VV} = \frac{2+r_L^2}{(2+r_L)^2}\,, \tag{22}$$

with $r_L = (1-\epsilon_V^2/2)^2$ from the longitudinal contribution.

The spin factor for each decay channel is shown in Fig. 1. For $m_h < 2m_V$, $\mathcal{P}_{VV}$ is smaller than 1/2, which reduces its weight compared to fermion channels. At the threshold $m_h = 2m_V$, the two- and three-body descriptions coincide and yield $\mathcal{P}_{VV} = 1/3$. Near threshold, the vector bosons are non-relativistic, suppressing helicity information and equalizing contributions from all three helicities. In the heavy-Higgs limit, the vector bosons are highly boosted, and the longitudinal polarization dominates, so $\mathcal{P}_{VV}\to 1$. The channels to $f\bar{f}$, gg, $\gamma\gamma$ and $Z\gamma$ have $\mathcal{P}_i = 1/2$, since these particles carry two helicities, whereas the longitudinal mode of Z does not contribute.

NEAR-MAXIMAL EE IN HIGGS DECAYS

With the spin factors $\mathcal{P}_i$ determined, we calculate the EE for fixed SM inputs. Higgs BRs are taken from `HDECAY` [54, 55], including only to the three-body modes for $VV^{(*)}$. We also get an independent analytic calculation of partial widths (App. B) which gives consistent EE results (App. C).

In Fig. 2, the left panel shows the dependence of the EE on the Higgs mass, with other couplings and the SM vev fixed. A global maximum EE globally gives

$$m_h = 126.08 \pm 0.28 \text{ GeV}, \tag{23}$$

where the 1σ uncertainty is obtained from a Monte Carlo scan over all other SM parameters within their 1σ ranges [56] and the theory uncertainty for BRs [57, 58]. This is within 0.8% of the latest ATLAS result, 125.11 ± 0.11 GeV [59], and CMS result, 125.08 ± 0.12 GeV [60]. We can define a near-maximal region by

$$\frac{\Delta EE}{EE_{\rm max}} \equiv \frac{|EE(\rho_R)-EE_{\rm max}|}{EE_{\rm max}} < 0.1\%, \tag{24}$$

the observed Higgs mass lies within this band.

The right panel of Fig. 2 shows the EE as a function of m_W, with other parameters (including $U(1)_Y$ coupling g') fixed. Equivalently, the EE can be viewed as a function of the $SU(2)_L$ coupling g or the weak mixing angle $\sin\theta_W$. The global maximum EE selects

$$m_W = 80.506 \pm 0.376\,\text{GeV}\,, \tag{25}$$

where the 1σ error again reflects SM parameter and theory input uncertainties. The central value differs from the measured m_W by $< 0.17\%$. The corresponding near-maximal-EE band for m_W is considerably broader than input uncertainties.

In Fig. 3, we use the two-parameter κ framework [61] to probe the impact of Higgs-coupling deviations, representative of beyond-SM scenarios such as two-Higgs-doublet models [62]. We rescale the SM Higgs couplings as $g_{hVV}\to\kappa_V\times g^{\rm SM}_{hVV}$ and $g_{hff}\to\kappa_f\times g^{\rm SM}_{hff}$, keeping fermion and vector-boson masses fixed. The figure shows the EE in the (κ_f,κ_V) plane with all other parameters

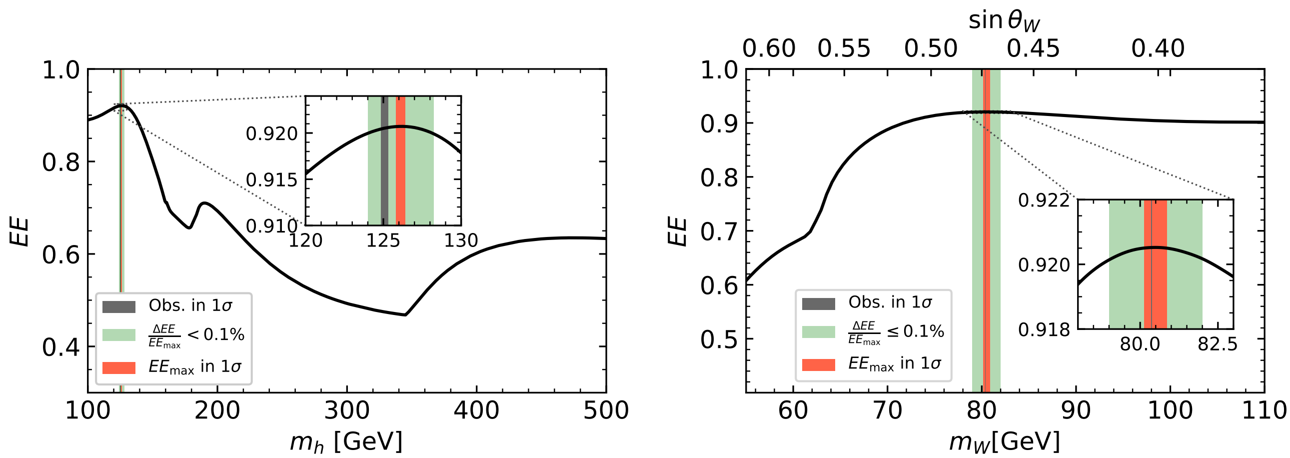

FIG. 2. Entanglement entropy of Higgs decays as a function of the Higgs mass (left) and m_W (right). The gray band marks the experimentally observed SM values (1σ), the red band shows the $EE_{\max}$ yield with its 1σ uncertainty from SM inputs and theory, and the green band indicates the near-maximal-EE region.

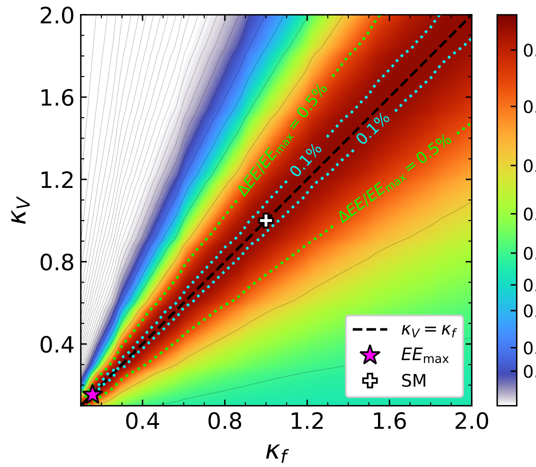

FIG. 3. EE in the κ_f–κ_V plane. Green and cyan dotted curves show contours of $\Delta EE/EE_{\max} = 0.5\%$ and 0.1%, respectively. The magenta star marks the maximal-EE point, and the white cross denotes the SM point.

at their SM values. The cyan contours denote the near-maximal condition $\Delta EE/EE_{\max} \leq 0.1\%$, which implies

$$\frac{\kappa_V}{\kappa_f} = 1.00^{+0.08}_{-0.06}\,. \tag{26}$$

Thus, the maximal-EE criterion prefers an approximately SM-like balance between hVV and hff couplings. As expected for observables built from BRs, the result is largely insensitive to an overall common rescaling of the couplings.

DISCUSSIONS

We now clarify several conceptual and practical choices in our analysis. Firstly, as a comparison we also tested an EE constructed from a purely diagonal "branching-ratio density matrix" $\rho_{\rm br} = \sum_i {\rm BR}_i\,|i\rangle\,\langle i|$, with i running over all decay channels. This gives $EE(\rho_{\rm br}) = 1-\sum_i {\rm BR}_i^2$ and leads to $m_h \sim 135$ GeV, an incorrect $m_W \sim 72$ GeV, and $\kappa_V/\kappa_f \sim 1.6$, as shown in Fig. 5 of App. D. These values are far from the observed SM results, underscoring that naive BR-based information is not sufficient and that the spin- and color–derived weights $\mathcal{P}_i/N_c^i$ are essential.

Secondly, as another baseline we evaluate the asymptotic Gibbs-Shannon entropy $S_\infty \sim \sum_i \log {\rm BR}_i$ of the classical multinomial distribution of Higgs decay counts used in Ref. [32]. We crosschecked that it selects $m_h \sim 126.52\pm0.09$ GeV and $m_W \sim 81.86\pm0.15$ GeV, close but not fully consistent with the SM value, together with a sizable deviation in $\kappa_V/\kappa_f = 1.3^{+0.2}_{-0.2}$, as shown in Fig. 6 of App. E. Since this construction uses only classical branching ratios, we regard it as a corroborating check rather than a substitute for our entanglement-based approach.

Third, we performed a preliminary study of W and Z decays with unpolarized initial states. For W decays, the $SU(2)_L$ gauge coupling drops out of the EE, leaving only CKM factors and fermion masses; the extremum is essentially flat and does not provide a clear inference. For Z decays, the EE does depend on $\sin\theta_W$, but the preferred value is significantly displaced from the SM one, as shown in Fig. 7 of App. F. By contrast, Higgs decays are more informative, since they simultaneously probe the scalar self-coupling, gauge couplings, and Yukawa couplings. Taken together, these observations tentatively suggest that EE in decay processes is most powerful when it captures *global* information across different sectors, and may be less discriminating within a single sector alone; alternative quantum-information measures beyond EE might be needed there.

Fourth, we deliberately trace out all kinematics at the outset rather than assigning $\mathcal{H}^{a}_{\rm kin}$ to $\mathcal{H}_A$ for a "symmetric" bipartition. With plane-wave states, a symmetric split leaves explicit box–normalization factors $\mathcal{V}$ from $\delta^{(3)}(\mathbf{0})$ and T from $\delta(0)$ in the EE. In practice, the volume/time dependence differs between two-body decays ($\propto T/\mathcal{V}$) and three-body decays ($\propto 1/\mathcal{V}$). Thus, the EE diverges or vanishes as $T,\mathcal{V}\to\infty$, and "normalizing" procedures [22] does not cure the mismatch. By tracing out kinematics, the reduced density matrix ρ_R is finite-dimensional (spin, color, species), and the EE is free of $\mathcal{V}$ and T. Thus, this bipartition is the well-posed choice.

Finally, we note that the off-shell four-body decays $h\to V^*V^*\to 4f$ are neglected: they are numerically subleading to the three-body VV^* channels, `HDECAY` does not include the full WW/ZZ and identical-fermion interference, and our construction of $\mathcal{P}_i$ would mix WW and ZZ channels in ρ_R and require an ambiguous fermion partition for four-body final states.

CONCLUSIONS

We explore the decay out-states of unstable particles as an intrinsic quantum-information probe of the SM parameter space, formulating an entanglement-entropy observable and applying it to SM Higgs decays. With spin– and color–entanglement weights included, a near-maximal-EE criterion selects a Higgs mass and W mass close to their measured values, and in a two-parameter κ framework it prefers an approximately SM-like balance $\kappa_V/\kappa_f\sim 1$. Comparisons with purely branching-ratio–based constructions and with multinomial Shannon entropy show that entanglement weights are essential for obtaining phenomenologically viable inferences. Preliminary W/Z studies further suggest that decay EE is most informative when it probes *global* scalar–gauge–Yukawa structure, and may be less discriminating within a single sector alone. Taken together, these results point to entanglement extremality in decay out-states as a compact, data-adjacent probe of SM couplings, and they motivate exploring complementary quantum-information measures beyond the EE when extending this program to other unstable particles.

Acknowlegements. The authors would like to thank Yuxin He and Jian Wang for helpful discussions. The work of J.L. is supported by the National Science Foundation of China under Grant No. 12235001, No. 12475103 and State Key Laboratory of Nuclear Physics and Technology under Grant No. NPT2025ZX11. The work of X.P.W. is supported by the National Science Foundation of China under Grant No. 12375095, and the Fundamental Research Funds for the Central Universities. The work of J.-J. Z. is supported by the National Science Foundation of China under Grants No. 11635001, 11875072. J.L. and X.P.W. also thank APCTP, Pohang, Korea, for their hospitality during the focus program [APCTP-2025-F01], from which this work greatly benefited. The authors gratefully acknowledge the valuable discussions and insights provided by the members of the Collaboration of Precision Testing and New Physics.

---

* jialiu@pku.edu.cn
† tanaka@pku.edu.cn
‡ hcwangxiaoping@buaa.edu.cn
§ zhang_jingjun@stu.pku.edu.cn
¶ zifanzheng@pku.edu.cn

[1] J. S. Bell, *On the Einstein-Podolsky-Rosen paradox*, *Physics Physique Fizika* **1** (1964) 195.

[2] A. J. Barr, M. Fabbrichesi, R. Floreanini, E. Gabrielli and L. Marzola, *Quantum entanglement and Bell inequality violation at colliders*, *Prog. Part. Nucl. Phys.* **139** (2024) 104134 [2402.07972].

[3] ATLAS collaboration, *Observation of quantum entanglement with top quarks at the ATLAS detector*, *Nature* **633** (2024) 542 [2311.07288].

[4] CMS collaboration, *Observation of quantum entanglement in top quark pair production in proton–proton collisions at $\sqrt{s}=13$ TeV*, *Rept. Prog. Phys.* **87** (2024) 117801 [2406.03976].

[5] Y. Afik et al., *Quantum information meets high-energy physics: input to the update of the European strategy for particle physics*, *Eur. Phys. J. Plus* **140** (2025) 855 [2504.00086].

[6] J. Lykken, *Quantum Information for Particle Theorists*, *PoS* **TASI2020** (2021) 010 [2010.02931].

[7] Y. Afik and J. R. M. de Nova, *Quantum information with top quarks in QCD*, *Quantum* **6** (2022) 820 [2203.05582].

[8] A. Cervera-Lierta, J. I. Latorre, J. Rojo and L. Rottoli, *Maximal Entanglement in High Energy Physics*, *SciPost Phys.* **3** (2017) 036 [1703.02989].

[9] G. M. Quinta, A. Sousa and Y. Omar, *Predicting leptonic CP violation via minimization of neutrino entanglement*, 2207.03303.

[10] J. Thaler and S. Trifinopoulos, *Flavor patterns of fundamental particles from quantum entanglement?*, *Phys. Rev. D* **111** (2025) 056021 [2410.23343].

[11] Q. Liu, I. Low and Z. Yin, *A Quantum Computational Determination of the Weak Mixing Angle in the Standard Model*, 2509.18251.

[12] S. R. Beane, D. B. Kaplan, N. Klco and M. J. Savage, *Entanglement Suppression and Emergent Symmetries of Strong Interactions*, *Phys. Rev. Lett.* **122** (2019) 102001 [1812.03138].

[13] I. Low and T. Mehen, *Symmetry from entanglement suppression*, *Phys. Rev. D* **104** (2021) 074014 [2104.10835].

[14] Q. Liu, I. Low and T. Mehen, *Minimal entanglement and emergent symmetries in low-energy QCD*, *Phys.*

Rev. C **107** (2023) 025204 [2210.12085].

[15] M. Carena, I. Low, C. E. M. Wagner and M.-L. Xiao, *Entanglement suppression, enhanced symmetry, and a standard-model-like Higgs boson*, *Phys. Rev. D* **109** (2024) L051901 [2307.08112].

[16] Q. Liu and I. Low, *Hints of entanglement suppression in hyperon-nucleon scattering*, *Phys. Lett. B* **856** (2024) 138899 [2312.02289].

[17] T.-R. Hu, S. Chen and F.-K. Guo, *Entanglement suppression and low-energy scattering of heavy mesons*, *Phys. Rev. D* **110** (2024) 014001 [2404.05958].

[18] S. Chang and G. Jacobo, *Consequences of minimal entanglement in bosonic field theories*, *Phys. Rev. D* **110** (2024) 096020 [2409.13030].

[19] K. Kowalska and E. M. Sessolo, *Entanglement in flavored scalar scattering*, *JHEP* **07** (2024) 156 [2404.13743].

[20] N. McGinnis, *Symmetry, entanglement, and the S-matrix*, 2504.21079.

[21] G. Busoni, J. Gargalionis, E. N. V. Wallace and M. J. White, *Emergent symmetry in a two-Higgs-doublet model from quantum information and nonstabilizerness*, *Phys. Rev. D* **112** (2025) 035022 [2506.01314].

[22] J. Liu, M. Tanaka, X.-P. Wang, J.-J. Zhang and Z. Zheng, *Scattering entanglement entropy and its implications for electroweak phase transitions*, *Phys. Rev. D* **112** (2025) 015028 [2505.06001].

[23] M. Carena, G. Coloretti, W. Liu, M. Littmann, I. Low and C. E. M. Wagner, *Entanglement maximization and mirror symmetry in two-Higgs-doublet models*, *JHEP* **08** (2025) 016 [2505.00873].

[24] T.-R. Hu, K. Sone, F.-K. Guo, T. Hyodo and I. Low, *Entanglement Suppression, Quantum Statistics and Symmetries in Spin-3/2 Baryon Scatterings*, 2506.08960.

[25] C. Núñez, M. Pardina, M. Asorey, J. I. Latorre and A. Cervera-Lierta, *Gauge invariance from quantum information principles*, 2511.04358.

[26] N. McGinnis, *Crossing Symmetry and Entanglement*, 2511.10559.

[27] ATLAS collaboration, *A detailed map of Higgs boson interactions by the ATLAS experiment ten years after the discovery*, *Nature* **607** (2022) 52 [2207.00092].

[28] CMS collaboration, *A portrait of the Higgs boson by the CMS experiment ten years after the discovery.*, *Nature* **607** (2022) 60 [2207.00043].

[29] M. Shaposhnikov and C. Wetterich, *Asymptotic safety of gravity and the Higgs boson mass*, *Phys. Lett. B* **683** (2010) 196 [0912.0208].

[30] C. D. Froggatt and H. B. Nielsen, *Standard model criticality prediction: Top mass 173 +- 5-GeV and Higgs mass 135 +- 9-GeV*, *Phys. Lett. B* **368** (1996) 96 [hep-ph/9511371].

[31] G. Degrassi, S. Di Vita, J. Elias-Miro, J. R. Espinosa, G. F. Giudice, G. Isidori et al., *Higgs mass and vacuum stability in the Standard Model at NNLO*, *JHEP* **08** (2012) 098 [1205.6497].

[32] A. Alves, A. G. Dias and R. da Silva, *Maximum Entropy Principle and the Higgs Boson Mass*, *Physica A* **420** (2015) 1 [1408.0827].

[33] A. J. Barr, *Testing Bell inequalities in Higgs boson decays*, *Phys. Lett. B* **825** (2022) 136866 [2106.01377].

[34] M. Fabbrichesi, R. Floreanini and E. Gabrielli, *Constraining new physics in entangled two-qubit systems: top-quark, tau-lepton and photon pairs*, *Eur. Phys. J. C* **83** (2023) 162 [2208.11723].

[35] J. A. Aguilar-Saavedra, A. Bernal, J. A. Casas and J. M. Moreno, *Testing entanglement and Bell inequalities in $H \to ZZ$*, *Phys. Rev. D* **107** (2023) 016012 [2209.13441].

[36] J. A. Aguilar-Saavedra, *Laboratory-frame tests of quantum entanglement in $H \to WW$*, *Phys. Rev. D* **107** (2023) 076016 [2209.14033].

[37] R. Ashby-Pickering, A. J. Barr and A. Wierzchucka, *Quantum state tomography, entanglement detection and Bell violation prospects in weak decays of massive particles*, *JHEP* **05** (2023) 020 [2209.13990].

[38] M. M. Altakach, P. Lamba, F. Maltoni, K. Mawatari and K. Sakurai, *Quantum information and CP measurement in $H \to \tau+\tau-$ at future lepton colliders*, *Phys. Rev. D* **107** (2023) 093002 [2211.10513].

[39] M. Fabbrichesi, R. Floreanini, E. Gabrielli and L. Marzola, *Bell inequalities and quantum entanglement in weak gauge boson production at the LHC and future colliders*, *Eur. Phys. J. C* **83** (2023) 823 [2302.00683].

[40] A. Bernal, P. Caban and J. Rembieliński, *Entanglement and Bell inequalities violation in $H \to ZZ$ with anomalous coupling*, *Eur. Phys. J. C* **83** (2023) 1050 [2307.13496].

[41] K. Ma and T. Li, *Testing Bell inequality through $\boldsymbol{h \to \tau\tau}$ at CEPC**, *Chin. Phys. C* **48** (2024) 103105 [2309.08103].

[42] J. A. Aguilar-Saavedra, *Tripartite entanglement in $H \to ZZ, WW$ decays*, *Phys. Rev. D* **109** (2024) 113004 [2403.13942].

[43] A. Bernal, P. Caban and J. Rembieliński, *Entanglement and Bell inequality violation in vector diboson systems produced in decays of spin-0 particles*, *Sci. Rep.* **15** (2025) 23410 [2405.16525].

[44] M. Del Gratta, F. Fabbri, P. Lamba, F. Maltoni and D. Pagani, *Quantum properties of $H \to VV^*$: precise predictions in the SM and sensitivity to new physics*, *JHEP* **09** (2025) 013 [2504.03841].

[45] D. Gonçalves, A. Kaladharan and A. Navarro, *Higher-Order Corrections to Quantum Observables in $h \to WW^*$*, 2506.19951.

[46] P. Bechtle, C. Breuning, H. K. Dreiner and C. Duhr, *A critical appraisal of tests of locality and of entanglement versus non-entanglement at colliders*, 2507.15947.

[47] S. A. Abel, H. K. Dreiner, R. Sengupta and L. Ubaldi, *Colliders are Testing neither Locality via Bell's Inequality nor Entanglement versus Non-Entanglement*, 2507.15949.

[48] L. Lello, D. Boyanovsky and R. Holman, *Entanglement entropy in particle decay*, *JHEP* **11** (2013) 116 [1304.6110].

[49] S. Seki, I. Y. Park and S.-J. Sin, *Variation of Entanglement Entropy in Scattering Process*, *Phys. Lett. B* **743** (2015) 147 [1412.7894].

[50] P. Zanardi, C. Zalka and L. Faoro, *Entangling power of quantum evolutions*, *Phys. Rev. A* **62** (2000) 030301 [quant-ph/0005031].

[51] I. Low and Z. Yin, *Elastic cross section is entanglement entropy*, *Phys. Rev. D* **111** (2025) 065027 [2410.22414].

[52] All channels involve the same type particle pair except the $Z\gamma$ mode. The $Z\gamma$ channel would introduce cross-channel interference terms in Eq. (13). Since $\mathrm{BR}_{Z\gamma}$ is negligible, we ignore these terms and treat

Eq. (13) as exact.

[53] W.-Y. Keung and W. J. Marciano, *HIGGS SCALAR DECAYS: H —> W+- X*, *Phys. Rev. D* **30** (1984) 248.

[54] A. Djouadi, J. Kalinowski and M. Spira, *HDECAY: A Program for Higgs boson decays in the standard model and its supersymmetric extension*, *Comput. Phys. Commun.* **108** (1998) 56 [hep-ph/9704448].

[55] HDECAY collaboration, *HDECAY: Twenty$_{++}$ years after*, *Comput. Phys. Commun.* **238** (2019) 214 [1801.09506].

[56] Particle Data Group collaboration, *Review of particle physics*, *Phys. Rev. D* **110** (2024) 030001.

[57] LHC Higgs Cross Section Working Group collaboration, *Handbook of LHC Higgs Cross Sections: 4. Deciphering the Nature of the Higgs Sector*, *CERN Yellow Rep. Monogr.* **2** (2017) 1 [1610.07922].

[58] E. Bagnaschi, L. Biermann and M. Spira, *Higgs-Boson Decays: Updates*, 10, 2025, 2510.24658.

[59] ATLAS collaboration, *Combined Measurement of the Higgs Boson Mass from the $H\to\gamma\gamma$ and $H\to ZZ^*\to 4\ell$ Decay Channels with the ATLAS Detector Using s=7, 8, and 13 TeV pp Collision Data*, *Phys. Rev. Lett.* **131** (2023) 251802 [2308.04775].

[60] CMS collaboration, *Measurement of the Higgs boson mass and width using the four-lepton final state in proton-proton collisions at s=13 TeV*, *Phys. Rev. D* **111** (2025) 092014 [2409.13663].

[61] LHC Higgs Cross Section Working Group collaboration, *Handbook of LHC Higgs Cross Sections: 3. Higgs Properties*, 1307.1347.

[62] G. C. Branco, P. M. Ferreira, L. Lavoura, M. N. Rebelo, M. Sher and J. P. Silva, *Theory and phenomenology of two-Higgs-doublet models*, *Phys. Rept.* **516** (2012) 1 [1106.0034].

[63] A. Djouadi, *The Anatomy of electro-weak symmetry breaking. I: The Higgs boson in the standard model*, *Phys. Rept.* **457** (2008) 1 [hep-ph/0503172].

[64] M. Spira, *Higgs Boson Production and Decay at Hadron Colliders*, *Prog. Part. Nucl. Phys.* **95** (2017) 98 [1612.07651].

[65] J. Wang, X. Wang and Y. Wang, *Analytic decay width of the Higgs boson to massive bottom quarks at order α_s^3*, *JHEP* **03** (2025) 163 [2411.07493].

[66] J. Aparisi et al., *mb at mH: The Running Bottom Quark Mass and the Higgs Boson*, *Phys. Rev. Lett.* **128** (2022) 122001 [2110.10202].

[67] J. A. M. Vermaseren, S. A. Larin and T. van Ritbergen, *The 4-loop quark mass anomalous dimension and the invariant quark mass*, *Phys. Lett. B* **405** (1997) 327 [hep-ph/9703284].

[68] S. A. Larin and J. A. M. Vermaseren, *The Three loop QCD Beta function and anomalous dimensions*, *Phys. Lett. B* **303** (1993) 334 [hep-ph/9302208].

[69] T. van Ritbergen, J. A. M. Vermaseren and S. A. Larin, *The Four loop beta function in quantum chromodynamics*, *Phys. Lett. B* **400** (1997) 379 [hep-ph/9701390].

[70] J. R. Ellis, M. K. Gaillard and D. V. Nanopoulos, *A Phenomenological Profile of the Higgs Boson*, *Nucl. Phys. B* **106** (1976) 292.

[71] B. W. Lee, C. Quigg and H. B. Thacker, *Weak Interactions at Very High-Energies: The Role of the Higgs Boson Mass*, *Phys. Rev. D* **16** (1977) 1519.

[72] B. A. Kniehl, *Radiative corrections for $H\to W^+W^-$ (γ) in the standard model*, *Nucl. Phys. B* **357** (1991) 439.

[73] A. Bredenstein, A. Denner, S. Dittmaier and M. M. Weber, *Precise predictions for the Higgs-boson decay H —> WW/ZZ —> 4 leptons*, *Phys. Rev. D* **74** (2006) 013004 [hep-ph/0604011].

[74] M. A. Shifman, A. I. Vainshtein, M. B. Voloshin and V. I. Zakharov, *Low-Energy Theorems for Higgs Boson Couplings to Photons*, *Sov. J. Nucl. Phys.* **30** (1979) 711.

[75] R. N. Cahn, M. S. Chanowitz and N. Fleishon, *Higgs Particle Production by Z —> H Gamma*, *Phys. Lett. B* **82** (1979) 113.

[76] T. G. Rizzo, *Gluon Final States in Higgs Boson Decay*, *Phys. Rev. D* **22** (1980) 178.

[77] A. Denner, S. Dittmaier and A. Mück, *PROPHECY4F 3.0: A Monte Carlo program for Higgs-boson decays into four-fermion final states in and beyond the Standard Model*, *Comput. Phys. Commun.* **254** (2020) 107336 [1912.02010].

[78] J. F. Donoghue, E. Golowich and B. R. Holstein, *Dynamics of the standard model*, vol. 2. CUP, 2014, 10.1017/CBO9780511524370.

Appendix for
Parameter Inference from Final-State Entanglement in Higgs Decays

In this appendix, we provide detailed derivations and extended calculations supporting the results presented in the main text.

A. The spin factor in the off-shell decay $h \to VV^*$

We here describe the detail of the derivation of Eq. (17). For the process $h(p_{\rm in}) \to W(p_1)W^*(q) \to V(p_1)f(p_2)\bar{f}(p_3)$, the final state can be written as

$$|{\rm out}\rangle|_{h\to WW^*} = \sum_f \sum_{\lambda_1,\lambda_2,s_2,s_3} \int d\Phi_3(p_{\rm in},p_1,p_2,p_3)\mathcal{M}^{f,W}_{\lambda_1\lambda_2 s_2 s_3}(p_1,p_2,p_3)\,|\mathbf{p}_1,\lambda_1\rangle_V\,|\mathbf{p}_2,s_2,f\rangle\,|\mathbf{p}_3,s_3,f\rangle\ , \tag{27}$$

where the amplitude is given by [53]

$$\mathcal{M}^{f,W}_{\lambda_1\lambda_2 s_2 s_3}(p_1,p_2,p_3) = \mathcal{M}^{h\to WW^*}_{\lambda_1\lambda_2}(p_1,q)\frac{1}{q^2-m_W^2+im_W\Gamma_W}\mathcal{M}^{W^*\to f\bar{f}}_{\lambda_2 s_2 s_3}(p_2,p_3)\,, \tag{28}$$

$$\mathcal{M}^{h\to WW^*}_{\lambda_1\lambda_2}(p_1,q) = i\frac{2m_W^2}{v}g^{\mu\nu}\epsilon^*_\mu(p_1,\lambda_1)\epsilon^*_\nu(q,\lambda_2)\,, \tag{29}$$

$$\mathcal{M}^{W^*\to f\bar{f}}_{\lambda_2 s_2 s_3}(p_2,p_3) = -ig_2\epsilon_\rho(q,\lambda_2)\bar{u}_f(p_2,s_2)\gamma^\rho\left(\frac{1-\gamma_5}{2}\right)v_f(p_3,s_3)\,, \tag{30}$$

where $\epsilon(p,\lambda)$ is the polarization vector, and u_f and v_f are the fermion spinors. Although we explicitly keep the helicity state of the off-shell W^* boson labeled by λ_2, the expression can be simplified by using the well-known replacement $\sum_{\lambda_2}\epsilon_\rho(q,\lambda_2)\epsilon^*_\nu(q,\lambda_2) \to -g_{\rho\nu}+q_\rho q_\nu/q^2$. Using this replacement, the amplitude simplifies as $\sum_{\lambda_2}\mathcal{M}^{f,W}_{\lambda_1\lambda_2 s_2 s_3} \to \mathcal{M}^{f,W}_{\lambda_1 s_2 s_3}$, as shown in Eq. (17).

In deriving the reduced density matrix given in Eq. (9), we trace over the full fermionic final states as

$$\rho_R \ni \sum_{\tilde{f}}\sum_{s_1',s_2'}\int d\Pi_1 d\Pi_2 d\Pi_3\,\langle\mathbf{p}_1|_W\,\langle\mathbf{p}_2,\mathbf{p}_3;s_1',s_2',\tilde{f}|\,\rho_f\,|\mathbf{p}_1\rangle_W\,|\mathbf{p}_2,\mathbf{p}_3;s_1',s_2',\tilde{f}\rangle\ . \tag{31}$$

Performing the summations and integrals in Eq. (31), we obtain

$$\rho_R \ni \frac{1}{2m_h\Gamma_{\rm tot}}\sum_{\lambda_1,\lambda_1'}\int d\Phi_3(p_{\rm in},p_1,p_2,p_3)\mathcal{M}^{f,W}_{\lambda_1 s_1 s_2}(\mathcal{M}^{f,W}_{\lambda_1' s_1 s_2})^*\,|\lambda_1\rangle_W\,\langle\lambda_1'|_W = \sum_{\lambda_1,\lambda_1'}\frac{\Gamma^{WW}_{\lambda_1\lambda_1'}}{\Gamma_{\rm tot}}\,|\lambda_1\rangle_W\,\langle\lambda_1'|_W\ , \tag{32}$$

which is the same as Eq. (17) with $V=W$. An analogous calculation for the $h\to ZZ^*$ decay process leads to the same conclusion.

We then derive the expression of the spin factor $\mathcal{P}_i$ for the three-body decay process $h\to Vf\bar{f}$. For this decay process, $\mathcal{P}_i$ is given by

$$\mathcal{P}_i = \frac{\sum_{\lambda_1,\lambda_2}\Gamma^{VV}_{\lambda_1\lambda_2}\Gamma^{VV}_{\lambda_2\lambda_1}}{\left(\sum_{\lambda_1}\Gamma^{VV}_{\lambda_1\lambda_1}\right)^2}\,. \tag{33}$$

Therefore, we need to evaluate the decay width $\Gamma^{VV}_{\lambda_1\lambda_2}$ for each helicity state of the V boson. In the following, we derive the explicit expression of $\Gamma^{VV}_{\lambda_1\lambda_2}$.

For the three-body phase-space measure, we can use the decomposition

$$d\Phi_3(p_{\rm in},p_1,p_2,p_3) = \frac{dx}{2\pi}d\Phi_2(p_{\rm in}\to p_1,q)d\Phi_2(q\to p_2,p_3)\,, \tag{34}$$

with $x=q^2$. Then, the decay width $\Gamma^{VV}_{\lambda_1\lambda_2}$ can be expressed as

$$\Gamma^{VV}_{\lambda_1\lambda_3} = \frac{1}{2m_h}\sum_f\sum_{\lambda_2,\lambda_2',s_2,s_3}\int\frac{dx}{2\pi}d\Phi_2(p_1,q)\frac{\mathcal{M}^{h\to VV^*}_{\lambda_1\lambda_2}(\mathcal{M}^{h\to VV^*}_{\lambda_3\lambda_2'})^*}{(q^2-m_V^2)^2+m_V^2\Gamma_V^2}\int d\Phi_2(q\to p_2,p_3)\mathcal{M}^{V^*\to f\bar{f}}_{\lambda_2 s_2 s_3}(\mathcal{M}^{V^*\to f\bar{f}}_{\lambda_2' s_2 s_3})^* \tag{35}$$

$$= \frac{1}{2m_h}\sum_f\int\frac{dx}{2\pi}d\Phi_2\frac{k_V\,m_V^2}{(q^2-m_V^2)^2+m_V^2\Gamma_V^2}\epsilon^*_\mu(\lambda_1)\epsilon_\nu(\lambda_3)\left(g^{\mu\rho}-\frac{q^\mu q^\rho}{q^2}\right)\left(g^{\nu\sigma}-\frac{q^\nu q^\sigma}{q^2}\right)\int d\Phi_2 J^f_\rho J^f_\sigma\,, \tag{36}$$

where $J^f_\mu = \bar{u}_f(c^f_V - c^f_A\gamma^5)v_f$, and k_V is a constant which depends on the type of V boson. For the last integral, we can use the following useful relation

$$\sum_f \int d\Phi_2(q \to p_2, p_3) J^f_\rho J^f_\sigma = x A^V_T \left(-g_{\rho\sigma} + \frac{q_\rho q_\sigma}{q^2} \right) , \tag{37}$$

with

$$A^W_T \simeq \sum_f \frac{N^f_c}{12\pi} , \quad A^Z_T = \sum_f \frac{N^f_c \left[(c^f_V)^2 + (c^f_A)^2 \right]}{12\pi} . \tag{38}$$

As a result, we obtain

$$\begin{aligned} \Gamma^{VV}_{\lambda_1\lambda_2} =& \frac{1}{2m_h} \int \frac{dx}{2\pi} \int d\Phi_2(p_{\rm in} \to p_1, q) \frac{k_V m_V^2}{(q^2 - m_V^2)^2 + m_V^2\Gamma_V^2} x A^V_T \left[-\epsilon^*(\lambda_1)\cdot\epsilon(\lambda_2) + \frac{(\epsilon^*(\lambda_1)\cdot q)(\epsilon(\lambda_2)\cdot q)}{q^2} \right] \\ =& \frac{1}{2m_h} \int \frac{dx}{2\pi} \frac{k_V m_V^2}{(x - m_V^2)^2 + m_V^2\Gamma_V^2} x A^V_T \frac{\lambda^{1/2}(m_h^2, m_W^2, x)}{16\pi m_h^2} \Xi_{\lambda_1\lambda_2} , \end{aligned} \tag{39}$$

where

$$\lambda(a, b, c) = a^2 + b^2 + c^2 - 2ab - 2bc - 2ca . \tag{40}$$

The quantity $\Xi_{\lambda_1\lambda_2}$ satisfies the following equations for each helicity state

$$\Xi_{\pm\pm} = 1 , \quad \Xi_{00} = r_V(x) = \frac{(m_h^2 - m_V^2 - x)^2}{4m_V^2 x} , \quad \Xi_{ij} = 0 \quad (i \neq j) . \tag{41}$$

For simplicity, we ignore the decay width in the denominator of Eq. (39). This assumption is reasonable in the SM because $m_V \gg \Gamma_V$ [56]. Then, the spin factor $\mathcal{P}_i$ for the $h \to VV^*$ can be expressed as a function of the V boson mass and the Higgs boson mass:

$$\mathcal{P}^{3-\text{body}}_{VV} = \frac{2F_T^2(\epsilon_V) + F_L^2(\epsilon_V)}{[2F_T(\epsilon_V) + F_L(\epsilon_V)]^2} , \tag{42}$$

where

$$F_T(\epsilon_V) = \int_0^{f_{\max}} df \frac{f}{(f-1)^2} \sqrt{(\epsilon_V^2 - 1 - f)^2 - 4f} , \tag{43}$$

$$F_L(\epsilon_V) = \int_0^{f_{\max}} df \frac{1}{4(f-1)^2} (\epsilon_V^2 - 1 - f)^2 \sqrt{(\epsilon_V^2 - 1 - f)^2 - 4f} , \tag{44}$$

with $\epsilon_V = m_h/m_V > 1$ and $f_{\max} = (\epsilon_V - 1)^2$. Using the above result, we can confirm that $\lim_{\epsilon_V \to 2} \mathcal{P}^{3-\text{body}}_{VV} \to 1/3$, which corresponds to the threshold limit.

When the Higgs mass satisfies $m_h > 2m_V$, the on-shell decay process $h(p_{\rm in}) \to V(p_1)V(p_2)$ is allowed. In this case, the decay width is given by

$$\begin{aligned} \Gamma^{VV}_{\lambda_1\lambda_2} &= \frac{2m_V^4}{m_h v^2} \int d\Phi_2(p_{\rm in}, p_1, p_2) \left[-\epsilon^*(\lambda_1)\cdot\epsilon(\lambda_2) + \frac{(\epsilon^*(\lambda_1)\cdot p_2)(\epsilon(\lambda_2)\cdot p_2)}{p_2^2} \right] \\ &= \frac{m_V^4}{8\pi m_h^3 v^2} \lambda^{1/2}(m_h^2, m_V^2, m_V^2) \Xi_{\lambda_1\lambda_2} \end{aligned} \tag{45}$$

Therefore, the spin factor is given by

$$\mathcal{P}^{2-\text{body}}_{VV} = \left. \frac{2\Xi_{++}^2 + \Xi_{00}^2}{(2\Xi_{++} + \Xi_{00})^2} \right|_{x = m_V^2} = \frac{2 + r_V^2(m_V^2)}{[2 + r_V(m_V^2)]^2} . \tag{46}$$

Since $r_V(m_V^2) = 1$ in the case with $m_h = 2m_V$, we obtain $\mathcal{P}^{2-\text{body}}_{VV} = \mathcal{P}^{3-\text{body}}_{VV} = 1/3$ at the threshold point.

B. The analytical formulae for Higgs decay partial widths

The following formulae for Higgs decay widths are based on Ref. [63] (for recent progress on higher-order corrections, see, see Ref. [58, 64]).

- $h \to q\bar{q}$ except for top quarks [63]

$$\Gamma(h \to q\bar{q}) = \frac{3m_h}{8\pi v^2}\bar{m}_q^2(m_h)\left[1 + \Delta_{qq} + \Delta_h^2\right] , \tag{47}$$

with

$$\Delta_{qq} = 5.67\frac{\bar{\alpha}_S}{\pi} + (35.94 - 1.36N_f)\left(\frac{\bar{\alpha}_S}{\pi}\right)^2 + (164.17 - 25.77N_f + 0.26N_f^2)\left(\frac{\bar{\alpha}_S}{\pi}\right)^3 , \tag{48}$$

$$\Delta_h^2 = \left(\frac{\bar{\alpha}_S}{\pi}\right)^2\left[1.57 - \frac{2}{3}\log\frac{m_h^2}{m_t^2} + \frac{1}{9}\log^2\left(\frac{\bar{m}_q^2(m_h)}{m_h^2}\right)\right] , \tag{49}$$

where $\bar{m}_q(\mu)$, m_t, N_f, and $\bar{\alpha}_S = \alpha_S(m_h)$ are the $\overline{MS}$ quark mass of flavor q at the scale μ, the top-quark mass, quark generation numbers and the strong coupling constant at m_h, respectively. The state-of-the-art QCD corrections at α_s^3, including full quark-mass dependence, have recently been computed [65]. For the bottom quark, its mass at the Higgs mass scale has been measured at the LHC with a relatively large uncertainty [66]. In our analysis, we employ the renormalization group evolution for quark masses discussed in Ref. [67] with the following input values [56]

$$\bar{m}_b(\bar{m}_b) = 4.18 \pm 0.03\,\text{GeV} , \quad \bar{m}_c(\bar{m}_c) = 1.280 \pm 0.025\,\text{GeV} , \quad \bar{m}_s(2\,\text{GeV}) = 93.5 \pm 0.8\,\text{MeV} . \tag{50}$$

For the renormalization group evolution of α_S, it is described at the three-loop level by [68, 69]

$$\frac{\partial\alpha_S}{\partial\ln\mu^2} = -\beta_0\alpha_S^2 - \beta_1\alpha_S^3 - \beta_2\alpha_S^4 , \tag{51}$$

with

$$\beta_0 = 11 - \frac{2}{3}N_f , \quad \beta_1 = 102 - \frac{38}{3}N_f , \quad \beta_2 = \frac{2857}{2} - \frac{5033}{18}N_f + \frac{325}{54}N_f^2 . \tag{52}$$

For the input value in Eq. (51), we use $\alpha_S(m_Z) = 0.1180 \pm 0.0009$ [56].

- $h \to t\bar{t}$ [63]

$$\Gamma(h \to t\bar{t}) = \frac{3m_h}{8\pi v^2}m_t^2\beta_t^3\left[1 + \frac{4}{3}\frac{\alpha_S}{\pi}\Delta_H^t(\beta_t)\right] , \tag{53}$$

where $\beta_i = \sqrt{1 - 4m_i^2/m_h^2}$, and

$$\Delta_H^t(\beta) = \frac{1}{\beta}A(\beta) + \frac{1}{16\beta^3}(3 + 34\beta^2 - 13\beta^4)\log\left(\frac{1+\beta}{1-\beta}\right) + \frac{3}{8\beta^2}(7\beta^2 - 1) . \tag{54}$$

The function $A(\beta)$ is defined by

$$\begin{aligned} A(\beta) = {} & (1+\beta^2)\left[4\text{Li}_2\left(\frac{1-\beta}{1+\beta}\right) + 2\text{Li}_2\left(-\frac{1-\beta}{1+\beta}\right) - 3\log\left(\frac{1+\beta}{1-\beta}\right)\log\left(\frac{2}{1+\beta}\right) - 2\log\left(\frac{1+\beta}{1-\beta}\right)\log\beta\right] \\ & - 3\beta\log\left(\frac{4}{1-\beta^2}\right) - 4\beta\log\beta . \end{aligned} \tag{55}$$

where Li_2 is the Spence function.

- $h \to \ell\bar{\ell}$ [70]

$$\Gamma(h \to \ell\bar{\ell}) = \frac{m_h}{8\pi v^2}m_\ell^2\beta_\ell^3 . \tag{56}$$

- $h \to WW$ (On-shell) [71]

$$\Gamma(h \to WW) = \frac{g_2^2 m_h^3}{64\pi m_W^2}\sqrt{1-\frac{4m_W^2}{m_h^2}}\left(1-\frac{4m_W^2}{m_h^2}+12\frac{m_W^4}{m_h^4}\right) . \tag{57}$$

Radiative corrections in this process require inclusion of the soft-photon bremsstrahlung contribution to avoid infrared divergences [72]. Since tracing out the soft-photon states is non-trivial, we employ the above formula in our analysis in the region $m_h > 2m_W$.

- $h \to WW^*$ (Off-shell) [53]

$$\Gamma(h \to WW^*) = \frac{3g_2^4 m_h}{512\pi^3} F\left(\frac{m_W}{m_h}\right) , \tag{58}$$

with

$$F(x) = \frac{3(1-8x^2+20x^4)}{\sqrt{4x^2-1}}\arccos\left(\frac{3x^2-1}{2x^3}\right) - (1-x^2)\left(\frac{47}{2}x^2-\frac{13}{2}+\frac{1}{x^2}\right) - \frac{3}{2}(1-6x^2+4x^4)\ln x^2 . \tag{59}$$

In addition to the decay process $h \to VV^*$, the Higgs boson can also decay via two off-shell gauge bosons, $h \to V^*V^*$ [73]. These processes can modify $\mathrm{BR}(h \to VV)$ by a few percent [63, 73]. This effect is neglected in our analyses since it is numerically subdominant, `HDECAY` does not include the full WW/ZZ and identical-fermion interference, and our $\mathcal{P}_i$ construction would mix the WW and ZZ channels in ρ_R and introduce an ambiguous choice of fermion partition for four-body final states.

In addition, we treat the final–state fermions as massless. This is an excellent approximation in the SM: helicity–flip terms in the $V^* \to f\bar{f}'$ current are proportional to m_f, so both rate and polarization effects enter only at $O(m_f^2/m_V^2)$. For the bottom quark case, we obtain $(m_b/m_W)^2 \simeq 2.7\times10^{-3}$ with all other fermions much smaller, and phase–space corrections from finite m_f are of similar size. Since these effects are well below the quoted input-parameter uncertainties, $\Delta m_b/\bar{m}_b(\bar{m}_b) \sim 0.7\%$, the massless approximation is justified.

- $h \to ZZ$ (On-shell) [71]

$$\Gamma(h \to ZZ) = \frac{g_2^2 m_h^3}{128\pi m_Z^2}\sqrt{1-\frac{4m_Z^2}{m_h^2}}\left(1-\frac{4m_Z^2}{m_h^2}+12\frac{m_Z^4}{m_h^4}\right) . \tag{60}$$

- $h \to ZZ^*$ (Off-shell) [53]

$$\Gamma(h \to ZZ^*) = \frac{g_2^4 m_h}{2048\pi^3\cos\theta_W^4}\left(7-\frac{40}{3}\sin\theta_W^2+\frac{160}{9}\sin\theta_W^4\right) F\left(\frac{m_Z}{m_h}\right) , \tag{61}$$

- $h \to \gamma\gamma$ [70, 74]

$$\Gamma(h \to \gamma\gamma) = \frac{\alpha_{\mathrm{EM}}^2}{256\pi^3 v^2} m_h^3 \left|\sum_f N_c^f Q_f^2 A_{1/2}(\tau_f) + A_1(\tau_W)\right|^2 , \tag{62}$$

where N_c^f is the color degrees of freedom for the fermion f, and

$$A_1(x) = 2+3x+3x(2-x)f(x) , \quad A_{1/2}(x) = -2x\left[1+(1-x)f(x)\right] , \tag{63}$$

with $\tau_X = 4m_X^2/m_h^2$, and

$$f(x) = \begin{cases} \arcsin^2(x^{-1/2}) & (x \le 1) \\ -\frac{1}{4}\left[\log\left(\frac{1+\sqrt{1-x}}{1-\sqrt{1-x}}\right) - i\pi\right]^2 & (x > 1) \end{cases} . \tag{64}$$

- $h \to Z\gamma$ [75]

$$\Gamma(h \to Z\gamma) = \frac{m_W^2 \alpha_{\rm EM} m_h^3}{128 v^4 \pi^4} \left(1 - \frac{m_Z^2}{m_h}\right)^3 \left| \sum_f N_f^c \frac{Q_f \hat{v}_f}{c_W} A_{1/2}(\tau_f, \lambda_f) + A_1(\tau_W, \lambda_W) \right|^2 \tag{65}$$

where $\lambda_i \equiv 4m_i^2/m_Z^2$, $\hat{v}_f = 2T_f^3 - 4Q_f s_W^2$, and

$$A_{1/2}(x,y) = I_1(x,y) - I_2(x,y)\,, \tag{66}$$

$$A_1(x,y) = c_W \left[4\left(3 - \frac{s_W^2}{c_W^2}\right) I_2(x,y) + \left\{ \left(1 + \frac{2}{x}\right) \frac{s_W^2}{c_W^2} - \left(5 + \frac{2}{x}\right) \right\} I_1(x,y) \right]\,, \tag{67}$$

with

$$I_1(x,y) = \frac{xy}{2(x-y)} + \frac{x^2 y^2}{2(x-y)^2} \left[f(x^{-1}) - f(y^{-1}) \right] + \frac{x^2 y}{(x-y)^2} \left[g(x^{-1}) - g(y^{-1}) \right]\,, \tag{68}$$

$$I_2(x,y) = -\frac{xy}{2(x-y)} \left[f(x^{-1}) - f(y^{-1}) \right]\,, \tag{69}$$

$$g(x) = \begin{cases} \sqrt{x^{-1} - 1} \arcsin \sqrt{x} & (x \geq 1) \\ \frac{\sqrt{1-x^{-1}}}{2} \left[\log\left(\frac{1+\sqrt{1-x^{-1}}}{1-\sqrt{1-x^{-1}}} \right) - i\pi \right] & (x < 1) \end{cases}\,. \tag{70}$$

- $h \to gg$ [76]

$$\Gamma(h \to gg) = \frac{\alpha_S^2 m_h^3}{72 v^2 \pi^3} \left| \frac{3}{4} \sum_q A_{1/2}(\tau_q) \right|^2\,. \tag{71}$$

C. Numerical results from analytic decay widths

To check consistency, we compare the EE obtained from `HDECAY` with that from the analytic expressions for the Higgs decay widths summarized in App. B.

In the upper panels of Fig. 4, the m_h and m_W dependence of the EE is shown. As seen in Fig. 4, there is a discrepancy between the `HDECAY` results (black solid line) and those from the analytic expressions for the Higgs decay widths (orange dashed line) due to higher-order corrections [55]. From the EE obtained using the analytic expressions for the Higgs decay widths, the predicted Higgs and W boson masses are

$$m_W = 79.726 \pm 0.148\,\text{GeV}\,, \quad m_h = 126.54 \pm 0.28\,\text{GeV}. \tag{72}$$

Comparing Eqs. (23) and (25), we conclude that higher-order corrections to the Higgs decay widths are important for obtaining precise predictions for the Higgs and W boson masses from the EE. In the lower panel of Fig. 4, the SM point (white cross) and the contour with $\kappa_f = \kappa_V$ (orange dashed line) lie in the near-maximal EE domain satisfying $\Delta EE/EE_{\rm max} \leq 0.1\%$. This is consistent with the result shown in Fig. 3.

D. Numerical results for $EE = 1 - \sum_i \mathrm{BR}_i^2$

We here show predicted SM parameters by maximizing the following simple EE

$$EE = 1 - \sum_i \mathrm{BR}_i^2\,. \tag{73}$$

This follows from the assumption that the reduced density matrix that traced out a certain partial state for the final state is given by

$$\rho_{\rm br} = \sum_i \mathrm{BR}_i \left| i \right\rangle \left\langle i \right|\,. \tag{74}$$

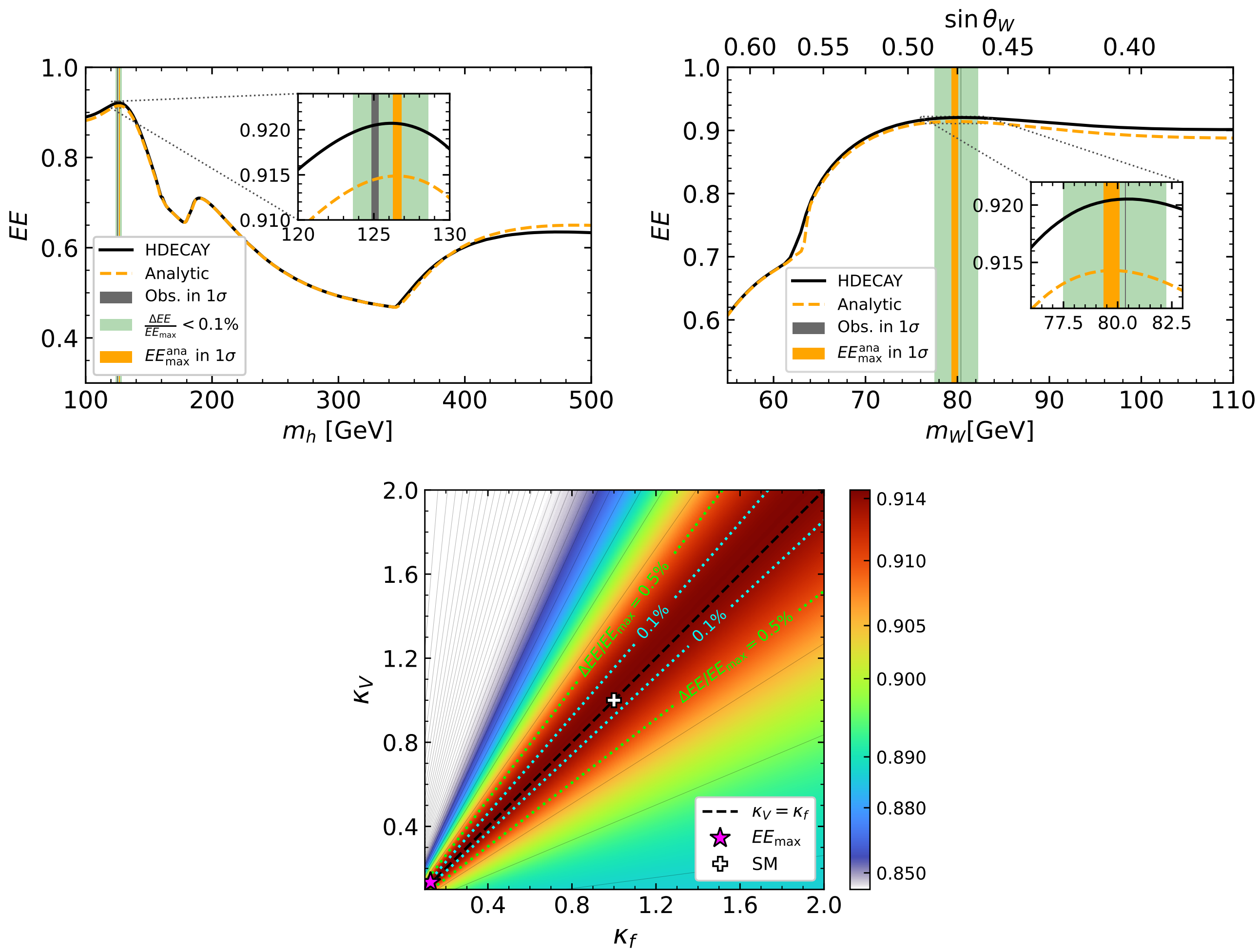

FIG. 4. Distributions of the entanglement entropy using analytical formulae for the Higgs decay widths. Upper left: Dependence of the EE on the Higgs mass m_h. The black solid line shows results from `HDECAY`, while the orange dashed line represents the EE calculated using analytical formulae. The orange band indicates $EE_{\max}$ with its 1σ uncertainty from SM inputs and theoretical uncertainties. Other colored codes follow the same definition as in Fig. 2. Upper right: Dependence of the EE on the W boson mass m_W. Bottom: EE distribution in the (κ_f, κ_V) plane.

It should be noted that the density matrix in Eq. (74) is of the block diagonal structure for each decay channel. Then, the purity is given by $\mathrm{tr}[\rho_{\rm br}^2] = \sum_i \mathrm{BR}_i^2$. Therefore, the linear entropy given in Eq. (10) can be expressed by Eq.(73).

In Fig. 5, the parameter dependence of the EE given in Eq. (73) is shown. Our analysis yields predicted Higgs and W boson masses below

$$m_W = 72.497 \pm 0.313\,\mathrm{GeV}\,, \quad m_h = 135.18 \pm 0.31\,\mathrm{GeV}. \tag{75}$$

Comparing Eqs. (23) and (25), it is concluded that Eq. (73) does not yield plausible predictions for the Higgs and W boson masses. Furthermore, the bottom panel of Fig. 5 shows that the SM point does not lie in a region of near-maximal EE. Based on these findings, we conclude that the EE defined by Eq. (73) is not applicable to the Higgs sector.

E. Results with the Gibbs-Shannon entropy

In our analysis, we have used the entanglement entropy (EE) defined in Eq.,(13) to calculate physical parameters such as the Higgs boson mass. In Ref. [32], demonstrated that the maximal classical multinomial entropy (Gibbs-Shannon entropy) provides a precise prediction for the Higgs boson mass. Here, we briefly explain their analysis and

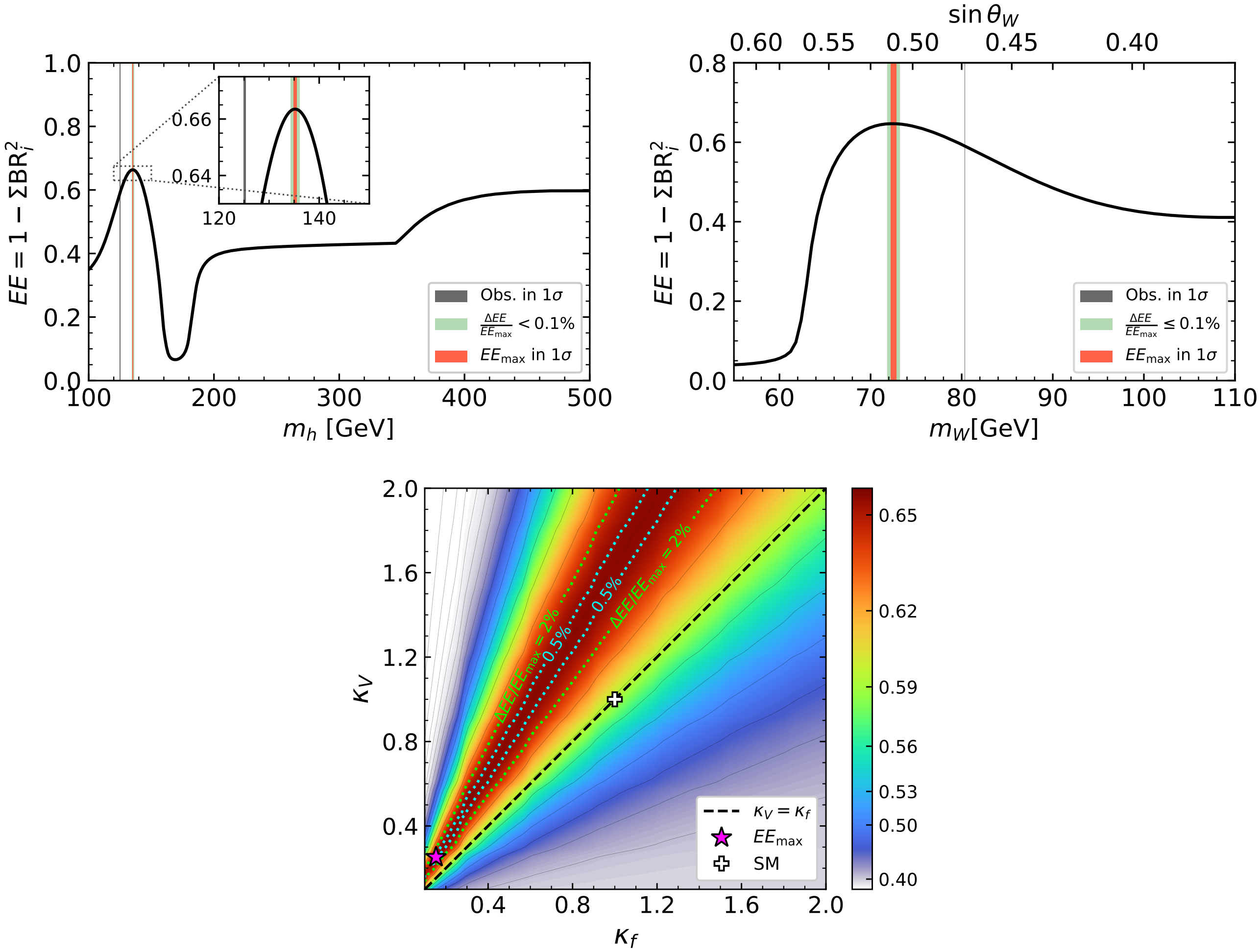

FIG. 5. Entanglement entropy distribution for Standard Model parameters using $EE = 1 - \sum_i \mathrm{BR}_i^2$. Upper left: EE as a function of Higgs mass m_h. Upper right: EE as a function of W boson mass m_W. Bottom: EE distribution in the (κ_f, κ_V) plane. Color coding follows the same convention as in Fig. 2.

the differences from our approach.

In classical information theory, probability distributions play a fundamental role. In Ref. [32], the decay branching ratios of the SM Higgs boson are treated as probabilities p_k for each channel k ($k = 1, \cdots, m$), and the Gibbs-Shannon entropy is evaluated. For N Higgs bosons, the Gibbs-Shannon entropy is given by [32]

$$S_N = \sum_{\{n\}}^{N} -P(\{n_k\}_{k=1}^m) \ln \left[P(\{n_k\}_{k=1}^m)\right] , \tag{76}$$

with

$$\sum_{\{n\}}^{N} \equiv \sum_{n_1=0}^{N} \cdots \sum_{n_m=0}^{N} \delta(N - \sum_{i=1}^{m} n_i) , \quad P(\{n_k\}_{k=1}^m) \equiv \frac{N!}{n_1! \cdots n_m!} \prod_{k=1}^{m} (p_k)^{n_k} , \tag{77}$$

where n_i indicates the number of Higgs bosons decaying into the channel i. The authors of Ref. [32] showed that S_N approaches a simple expression in the large-N limit (verified for $N > 10^7$):

$$S_\infty = \frac{1}{2} \ln \left[(2\pi N e)^{m-1} \prod_{k=1}^{m} p_k \right] + O\left(\frac{1}{N}\right) . \tag{78}$$

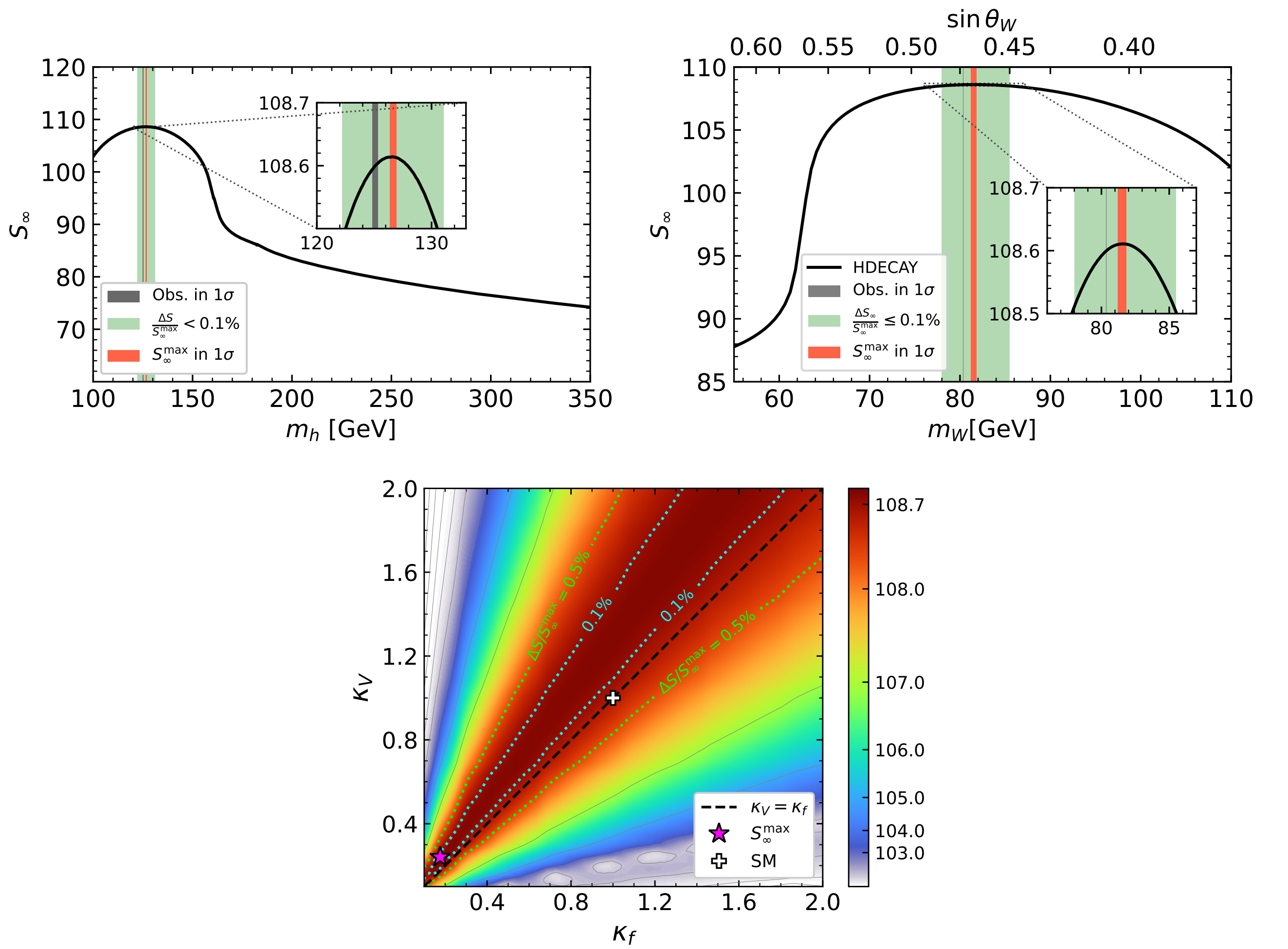

FIG. 6. Gibbs-Shannon entropy (Eq. (78)) as a function of Standard Model parameters. Upper left: Dependence on the Higgs mass m_h. Upper right: Dependence on the W boson mass m_W. Bottom: Distribution in the (κ_f, κ_V) plane. Color coding follows the same definition as in Fig. 2.

This implies that S_∞ is maximized when the decay processes are democratic ($p_1 = \cdots = p_m$), a property shared by the EE in Eq. (73).

The upper two panels of Fig. 6 show the dependence of the Gibbs-Shannon entropy on the Higgs and W boson masses. Following Ref. [32], we use $N = 10^9$ in our numerical calculations. We define the near-maximal entropy region (green domain) by $|S_\infty^{\max} - S_\infty|/S_\infty^{\max} \equiv \Delta S_\infty/S_\infty^{\max} \leq 0.1\%$. Maximizing S_∞ yields the following predictions for m_h and m_W:

$$m_h = 126.52 \pm 0.09\,\text{GeV}\,, \quad m_W = 81.856 \pm 0.148\,\text{GeV}\,. \tag{79}$$

The predicted Higgs mass deviates from the measured value by within 1.1%, consistent with our result in Eq. (23). The predicted W boson mass deviates by approximately 1.9% from the measured value. The bottom panel of Fig. 6 shows the Gibbs-Shannon entropy as a function of κ_f and κ_V. This figure reveals that the SM point and the contour $\kappa_f = \kappa_V$ lie outside the near-maximal entropy domain, despite the relatively accurate mass predictions shown in the upper panels. These findings suggest that the Gibbs-Shannon entropy in Eq. (78) cannot fully characterize the Higgs sector. Therefore, we conclude that the EE in Eq. (13) is more effective for determining Higgs properties and the structure of electroweak interactions.

We note that the predictions in Eq. (79) exclude 4-body decay channels $h \to V^*V^*$ for two reasons: (i) to maintain consistency with our previous analysis in Eqs. (23) and (25), where these subleading contributions were omitted; and (ii) because HDECAY, the computational tool used in both our work and Ref. [32], cannot adequately model these processes. For a proper treatment of 4-body final states, specialized tools like `PROPHECY4F` [77] would be required,

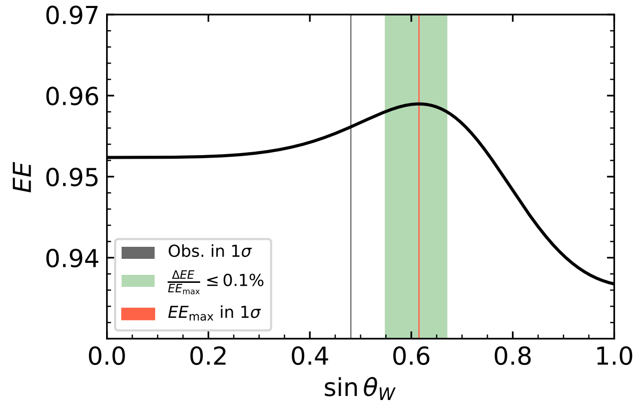

FIG. 7. Dependence of the entanglement entropy on the weak mixing angle for Z boson decays. Color regions follow the same convention as in Fig. 2.

which were not employed in the reference study. When these contributions are included using the ad hoc 4-body off-shell decay in HDECAY, our results agree with those of Ref. [32] within uncertainties.

F. The implication of EE in Z boson decay

We now apply our framework to Z boson decays. The Z boson decays into 11 channels: $Z \to f\bar{f}\,(f = q, \ell, \nu_e, \nu_\mu, \nu_\tau)$ except for top quarks. For an unpolarized initial Z boson, the leading-order decay width is given by [78]

$$\Gamma(Z \to f\bar{f}) = \frac{N_c^f g^2 m_Z}{48\pi \cos^2\theta_W}\left[c_V^2 + c_A^2 + 2(c_V^2 - 2c_A^2)\frac{m_f^2}{m_Z^2}\right]\sqrt{1 - \frac{4m_f^2}{m_Z^2}}\,, \tag{80}$$

where c_V and c_A are the vector and axial-vector couplings in the Zff vertex $-\frac{ig}{2\cos\theta_W}(c_V - c_A\gamma^5)$. Since the EE in Eq. (13) depends on branching ratios, it exhibits minimal dependence on the Z boson mass due to $m_f^2/m_Z^2 \ll 1$. We therefore investigate whether the EE for Z boson decays can predict the weak mixing angle $\sin\theta_W$.

To compute the EE in Eq. (13), we must determine the spin factor $\mathcal{P}_f$ for $Z \to f\bar{f}$. We begin by expressing the Zff vertex for each fermion as

$$-\frac{ig}{2\cos\theta_W}(c_V^f - c_A^f\gamma^5) = -\frac{ig}{\cos\theta_W}(g_L^f P_L + g_R^f P_R)\,, \tag{81}$$

where $c_{V,A}^f = g_L^f \pm g_R^f$, and $P_{L,R}$ are the chiral projection operators. From this vertex, we compute the decay width $\Gamma_{ij}^{\lambda_Z,f}$ for $Z \to f_i\bar{f}_j$, where λ_Z and i/j parameterize the polarization of the Z boson ($\lambda_Z = 0, \pm$) and helicity for fermions ($i, j = \pm$), respectively. The spin factor is then given by

$$\mathcal{P}_f^{\lambda_Z} = \frac{\sum_{ij}\Gamma_{ij}^{\lambda_Z,f}\Gamma_{ji}^{\lambda_Z,f}}{\left(\sum_{i,j}\Gamma_{ij}^{\lambda_Z,f}\right)^2}\,, \tag{82}$$

which can be expressed in terms of $g_{L/R}^f$ as

$$\mathcal{P}_f^{\pm} = \frac{(1-8x_f^4)\left[(g_L^f)^4 + (g_R^f)^4\right] + 2x_f^2(5-12x_f^2)\,(g_L^f g_R^f)^2 - 4x_f^2(1-4x_f^2)\,g_L^f g_R^f\left[(g_L^f)^2 + (g_R^f)^2\right]}{\left[(g_L^f)^2 + (g_R^f)^2\right]^2}\,, \tag{83}$$

$$\mathcal{P}_f^{0} = \frac{(1-8x_f^4)\left[(g_L^f)^4 + (g_R^f)^4\right] + 16x_f^2(1-3x_f^2)\,(g_L^f g_R^f)^2 + 8x_f^2(1-4x_f^2)\,g_L^f g_R^f\left[(g_L^f)^2 + (g_R^f)^2\right]}{\left[(g_L^f)^2 + (g_R^f)^2\right]^2}\,, \tag{84}$$

where $x_f = m_f/m_Z$. In the chiral limit ($x_f \to 0$), the spin factor is of the same form for all initial helicity: $\mathcal{P}_f^{\pm} = \mathcal{P}_f^0 = \left[(g_L^f)^4 + (g_R^f)^4\right]/\left[(g_L^f)^2 + (g_R^f)^2\right]^2$.

Fig. 7 shows the dependence of the EE on the weak mixing angle. The requirement of near-maximal EE yields

$$\sin\theta_W = 0.615^{+0.067}_{-0.056}\,, \tag{85}$$

which deviates from the measured value $\sin^2\theta_W(m_Z) = 0.231$ by approximately 28% [56]. We also performed a similar analysis for W boson decays, but found no meaningful results due to cancellations in the gauge coupling dependence of the EE. These findings suggest that decay processes involving global information in multiple sectors, such as Higgs boson decays, may be unique as the quantum information probes.